1 Introduction

The most important biological and environmental processes depend on the nature of interfacial water molecules and dissolved ions in boundary layers. Only in recent years, and through the development of surface-specific experimental[1–4] and computational[5–8] analytical techniques, have we been able to begin understanding this complex environment comprised of interfacial water and ions. The field has moved from studying simple water systems in vacuum, to studying ever more complex ones such as those near hydrophobic surfaces that are responsible for such important processes as ion transport, liquid-liquid extraction, drug delivery, and environmental remediation.

The computational studies presented herein have been conducted to augment recent experimental studies that showed how ions affect the interfacial region between an aqueous ionic solution and a hydrophobic liquid.[9] Classical molecular dynamics simulations have been performed to analyze the interface formed between various aqueous salt solutions and the organic liquid CCl_4 .Analyses were conducted for comparison with the salt solutions as well as for comparison with previous computational efforts.[10–15] Three salt solutions were simulated containing NaCl , $NaNO_3$, Na_2SO_4 . These were chosen for comparison to the recent experimental sum frequency generation (SFG) spectroscopy results for the same systems,[9] and to supplement those experiments with additional molecular-level information. Analyses were performed on the simulation data to extract ionic and molecular density data across organic interfaces, information about water orientation near the interfaces, and simulated SFG spectra.

The computational simulation results provide a microscopic molecular picture of the geometries and interactions occurring within these interfaces that is otherwise inaccessible with experimental methods. The conclusions drawn from the simulations are in excellent agreement with those of the experimental study, while going further to provide a detailed picture of how the density and orientation of interfacial water near the hydrophobic liquid surface is altered by the presence of different electrolyte ions, in the aqueous solution, that migrate into the interfacial region. Insights gained from these studies have important implications for understanding a host of environmental, biological, and technological processes involving water near hydrophobic surfaces.

1.1 Density Profiles

Density histograms of simulated interfaces have been used in previous publications to show ionic and molecular distribution behavior in various systems.[11,13,15–20] In this work the density profile of water throughout the interface is fitted to a hyperbolic tangent function[19,21] as shown here:

$$\rho(z) = \frac{1}{2}(\rho_1 + \rho_2) - \frac{1}{2}(\rho_1 - \rho_2)\tanh\left(\frac{z - z_0}{d}\right) \tag{1}$$

Equation (1) relates the interfacial density, ρ, as a function of position, z, along a given system reference axis, to the densities of the phases on either side of the location of the Gibb's dividing surface (GDS), z_0. The bulk density ρ_1 and the density within the second phase, ρ_2 are fitted. The interfacial width, d, is related to the "90-10" thickness that is often reported by $t_{90-10} = 2.197d$.

These measures of interfacial thickness provide a means of comparing the depths to which the water phase is affected by ions located at the interface. The density distributions of the salts depict concentration and depletion phenomena throughout the interfacial region, and also serve to illustrate ionic affinity within this region. Previous work has been performed on the air-water interface with ions of different levels of interfacial affinity, with the more polar ions being the most interfacially active.[3,20,22–27] We present the density distribution results below for the neat-H_2O and salt solutions adjacent to an organic CCl_4 phase.

1.2 Molecular Orientation

Several methods have been used previously to show molecular orientation profiles of water molecules throughout simulated interfacial regions.[5,10,11,19,28–32] Studies have utilized various internal coordinate definitions and a number of angle definitions, orientational order parameters, and probability distributions to relate molecular, or averaged, orientations. In this work we have chosen to compute the orientation of water using two vectors that intuitively describe the orientation in space, given the locations of the three atoms comprising the molecule. The molecular bisector, a vector that points along the axis of symmetry of the water molecule from the hydrogen-end to the oxygen, provides directional orientation similar to the water molecule's dipole. A second vector, that is referred to here as the molecular normal vector, is established as the vector pointing normal to the plane formed by the three atoms of the water molecule and establishes its planar "tilt". Analyzing the angle made between these two vectors and a given space-fixed reference axis (herein defined as the long-axis of the simulation cells, oriented perpendicular to the interfacial plane and pointing out of the aqueous phase) is a means of finding the orientation of waters within these simulated systems as illustrated in figure 1. The angle formed between the molecular bisector and the reference axis will hereafter be referred to as θ, and the molecular normal vector as ϕ. The analysis in this work reports the cosines of these two angles, and because of the symmetry of the water molecule where the hydrogens are not uniquely identified, the cosines of the two angles are limited as follows: $-1 \leq \cos\theta \leq 1$ and $0 \leq \cos\phi \leq 1$. We report the orientation profiles of θ and ϕ as functions of the distance from the GDS of the interface, as

found from the fitting in our density profile analyses.

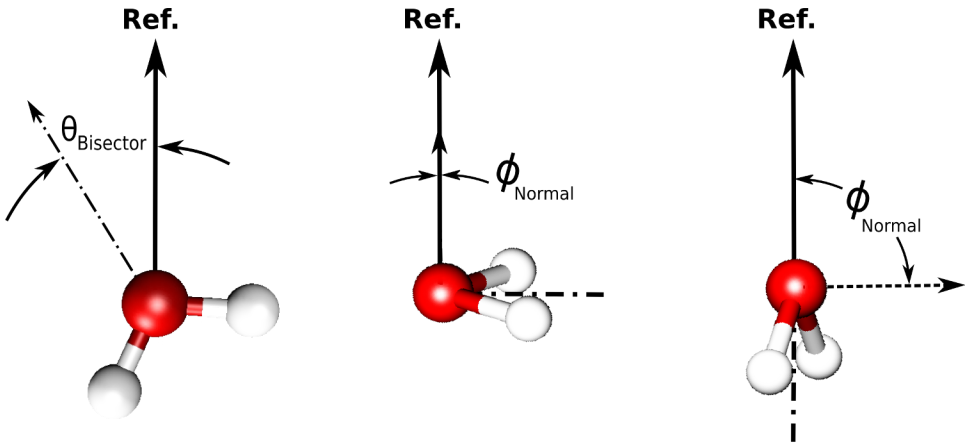

Figure. 1 — Angles used to define molecular orientation. The system reference (Ref.) axis is that which is perpendicular to the plane of the aqueous-organic interface, and points out from the aqueous phase into the organic one. The molecular bisector vector points from the hydrogen-end of the water to the oxygen end, and orients along the axis of symmetry. The angle it forms with the reference axis is either aligned or anti-aligned such that $-1 \leq \cos\theta \leq 1$. The angle formed between the vector normal to the molecular plane (formed by the three water atoms) and the reference-axis orients the "twist" of the molecule such that $0 \leq \cos\phi \leq 1$, where the water molecular plane is either laying flat on the interface ($\cos\phi = 1$) or it the water is perpendicular to the interface ($\cos\phi = 0$).

1.3 Computational SFG

A difficult challenge for experimental surface studies is in understanding the vibrational spectroscopy of liquid water. Hydrogen bonding between water molecules causes intermolecular and intra-molecular couplings. Simulations provide the analytical capacity to relate the broad lineshapes, and the often difficultly-assessed impact of hydrogen bonding as a function of OH vibrational frequency, to microscopic geometries, forces, and environments. In this work we compute the SFG spectra of the interface between the salt solutions and an organic phase to qualify the conclusions of a previous experimental work by our group,[9] and to elucidate some of the microscopic phenomena that lead to water's spectroscopic signatures.

The computational method used in this work is based on that of Morita and Hynes[33] as outlined in a previous study by this group utilizing the same technique.[34] The computational SFG technique has been improved in more recent studies by Morita et al,[35,36] and with other enhanced water models. The technique used in this work has been established to recreate qualitatively the experimental spectra to a sufficient degree such that we may draw qualified conclusions about lineshape and intensity.

2 Computational Method

The molecular dynamics methods used in this work are similar to those from our previous computational efforts with some modifications described below.[10,11,13] Simulations were carried out using the Amber 9 software package. The polarizable ion model parameters are taken from previous works on similar systems.[16,28,37–39] The polarizable POL3 model was used for water molecules.[40] Fully polarizable models have been used in previous interface simulation studies because they are known to more accurately reproduce interfacial structure and free energy profiles.[29,41–44]

A total of 4 systems were simulated consisting of aqueous salt and CCl_4 phases. A slab geometry was used to produce two interface regions within each simulation cell.[10] The results of the analyses performed herein on each simulated system made use of the natural symmetry of the two interfaces by averaging the results from the two surfaces. The organic region was formed in a box 30 Å on a side with 169 CCl_4 molecules to reproduce a standard temperature density of 1.59 $\frac{g}{mL}$. The aqueous region was formed in a box 30x30x60 Å ^{3}, with the long axis perpendicular to the interfaces. The number of water molecules and ions varied for each system in order to reproduce a concentration of 1.2 M. The specific populations of each molecule are listed in table 2. The organic and aqueous boxes were then joined to form a system 90 Å long with interface areas of 30x30 $\mathring{A}^2$.

System	H_2O	Cation	Anion
Neat Water	1800	0	0
NaCl	1759	40	40
$NaNO_3$	1732	40	40
Na_2SO_4	1740	86	43

Table 1 — Aqueous molecule and ion numbers. Listed are the populations of each component for the 4 simulated aqueous phases. All systems were simulated at near 1.2 M salt concentrations.

The water, salts, and CCl_4 were each randomly packed into their respective boxes with a minimum packing distance of 2.4 Å . After joining the aqueous and organic phases and forming the two interfaces, the total system was energy minimized using a conjugate gradient method. Following minimization, the system was equilibrated at a constant temperature of 298 K with weak coupling to a heat bath for a period of 10 ns, using a simulation timestep of 1.0 fs. A non-bonded potential cutoff of 9.0 Å was used. Following equilibration the system was simulated with the same parameters for a further 10 ns with atomic position data recorded every 50 fs. This resulted in a total of 200,000 snapshots which were used in the data analysis.

3 Component Densities

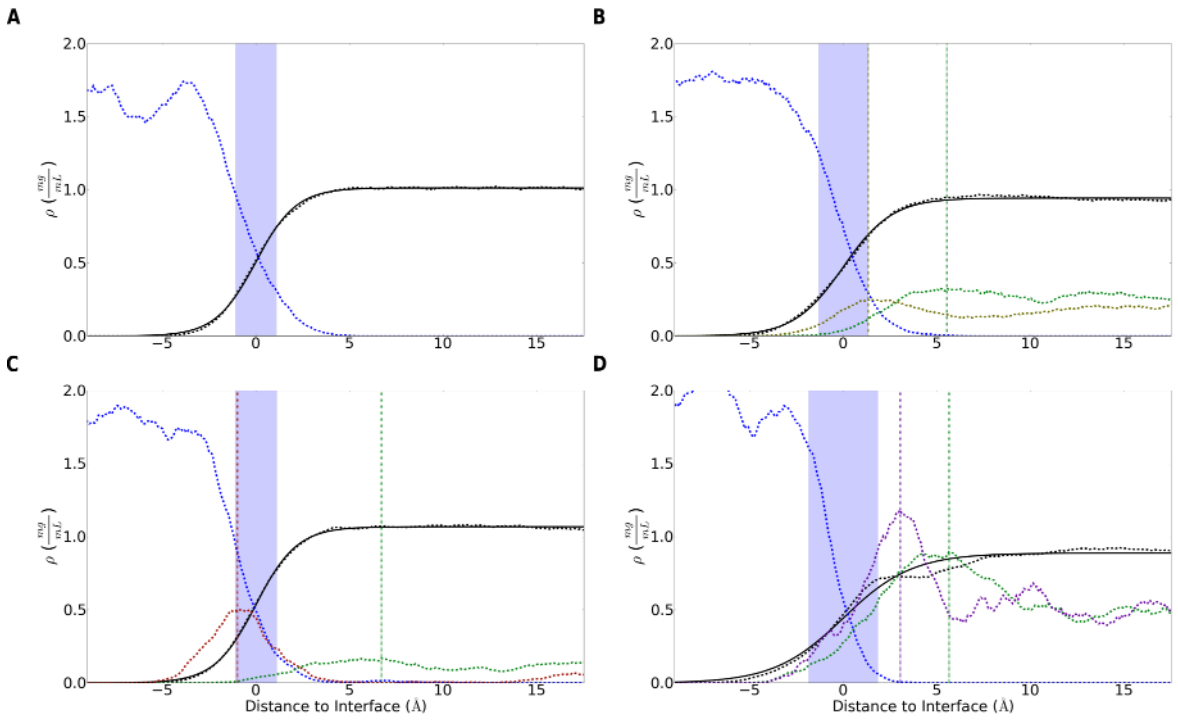

Figure. 2 — Aqueous salt solution (1.2 M) and CCl_4 surface density profiles. (A) Neat-H_2O, (B) NaCl, (C) $NaNO_3$, and (D) Na_2SO_4 aqueous solution densities are plotted with the water-oxygen density (dashed black) and the corresponding fitted lineshape (solid black). The CCl_4 (dashed blue), Na^+ cation (dashed green, scaled 10x) and respective anion (scaled 5x) densities are also shown for each system. The maxima of the ionic components are marked with dashed vertical lines of the same colors.

The component density profiles of each system were calculated to study the effects of added salts on water's density profile, and to find any deviations from the H_2O/CCl_4 system. The water density profile of each system was fitted to a hyperbolic tangent function (Eq. 1). The resulting plots are shown in figure 2. The profiles were centered about the GDS locations, z_0, at 0.0 Å , and all lineshapes are plotted as distances to the GDS. Each interfacial width, d, is designated as a highlighted blue region of width d centered about z_0. The widths of the interfacial regions for the neat-H_2O (A), NaCl (B), $NaNO_3$ (C), and Na_2SO_4 (D) systems are 2.16, 2.62, 2.20, 3.69 Å , respectively. In each of the salt solutions, the anion density profile shows higher density near the interface, appearing as a peak in the density profile. These anion enhancements all occur closer to the interface than the corresponding counter-cation. Various parameters of interest such as the interfacial thicknesses, ionic enhancement locations (taken to be the location of the maxima in the ion profiles), and relative distances between the peaks of the ion profiles are collected in table 2.

System	d	Anion	Cation	Anion-Cation Distance
Neat-H_2O	2.16	-	-	-
NaCl	2.62	1.33	5.53	4.20
$NaNO_3$	2.20	-0.99	6.71	7.70
Na_2SO_4	3.69	3.04	5.64	2.60

Table 2 — Aqueous salt system density parameters. Interfacial widths, d, and the locations of the maxima of the density profiles for each ionic component are listed for the simulated salt systems. The relative distances between the anion and cation density peak locations are listed to show how the different anions affect the relative location of their cationic counter-ions.

The oscillations in the surface density profiles of water and the adjoining organic CCl_4 liquid phase have been noted previously and attributed to thermal capillary waves on a larger length-scale than the simulated system size.[45] The same work also made note that the interfacial thickness is size-dependent on the interfacial surface area. Increasing the surface area dimensions should therefor cause a proportional increase in the interfacial width. As a consequence, care must be taken when making quantitative comparisons between widths and locations found in differing simulation studies. However, relative width ordering between similarly-sized systems should remain. Two works on the H_2O/CCl_4 surface offer direct comparison of this.[11,45]

In comparing the three salt solutions studied here, any differences in those systems are a result of the anion because the same cation was used in each system. NaCl is the simplest of the three salts with a monatomic and monovalent anion. The peak of the anion density profile is within the aqueous phase (i.e. it is found on the aqueous-side of the interfacial width). The location of the cation density peak is, as mentioned above, deeper into the aqueous phase than the anion by over 4 Å . This layering of ions within the aqueous phase is attributed to the break in the isotropy of the field of the bulk region upon introduction of the organic phase. The more polarizable and negatively charged anions move towards the interface to effectively screen the induced field from the organic phase. The counter-ions then are drawn towards the negative charge built up by the anions to create the second ion density peak deeper into the aqueous phase. The overall shape of the water profile in the NaCl system is relatively unaffected (compared to the neat-H_2O) by the presence of the ions. The bulk water density is unchanged, and the width of the interface is only slightly increased above that of neat-H_2O .

In an MD study by Wick and Dang[46] of H_2O/CCl_4 interfaces, larger and more polarizable monovalent anions were found to be less solvated and exhibited a smaller density enhancement when compared to the H_2O/air interface. The H_2O/CCl_4 interface was found to be a less favorable solvation environment for the more polarizable anions. A break in the isotropic environment around the ions causes them to be less solvated and come in greater contact with the CCl_4 phase. The ions are thus pushed further into the aqueous bulk than at an air-interface. However, the surface activities and ion density enhancements of the more polarizable anions (i.e. I^-, Br^-) remain greater than that of a smaller and less polarizable one (i.e.

Cl^-) at both interfaces.

We find from our density calculations that ions that increase the interfacial width at the H_2O/CCl_4 interface correspond to ions that result in an enhancing of the SFG signal from interfacial water. As discussed later, our SFG calculations show excellent agreement with experimental results. Also, we find those ions that are best known to enhance the strength of hydrogen-bonding (i.e. $SO_4{}^{2-}$) produce wider interfaces with greater water penetration into the CCl_4 phase.

The $NaNO_3$ system introduces the monovalent, polyatomic nitrate anion. In our simulation we find a strong surface density enhancement of the nitrate anion. The nitrate density peak is located the furthest out from the aqueous phase of the three salt systems, as expected by its higher polarizability and low charge. The location of the sodium cation peak in this system is a significant distance further into the bulk water from the anion than in either of the NaCl or Na_2SO_4 systems. The increase in ion-pair distance is likely the result of strong screening of the interfacial field by the surface-active anion, and the solvating waters around it. The interfacial width of the $NaNO_3$ system is the narrowest relative to the other salts in this study.

The widest interface is that of the Na_2SO_4 solution, indicating that the $SO_4{}^{2-}$ anions act to increase the number of interfacial water molecules on both sides of the GDS, consistent with the highly solvated nature of $SO_4{}^{2-}$ and its larger size. $SO_4{}^{2-}$ density enhancement (the peak of the anion density profile) is furthest into the aqueous bulk of the three anions simulated. The divalent and highly polarizable nature of the $SO_4{}^{2-}$ anion appears to attract its counter-ion closest, leading to the narrowest sub-surface ionic double-layer. This attraction is likely coulombic. Although the greatest anionic concentration enhancement is further into the bulk water region, seemingly outside the region designated by the interfacial width, the water interfacial width is still greatly enhanced. This is in agreement with the experimental Na_2SO_4 SFG studies where sulfate ion leads to an enhanced SFG signal throughout the bonded OH stretch region, consistent with a larger interfacial width.[9]

The majority of liquid surface studies examining ion behavior over the past decade have been conducted on H_2O/air interfaces. A review has been written that elucidates the convergence of data and conclusions regarding H_2O/air systems, paying special attention to relevant computational efforts.[47] Ion behavior at liquid-liquid interfaces, however, is clearly different than these air-water computational studies. The large polarizable and monovalent anions (Cl^- , Br^-, I^-) undergo concentration enhancement above bulk levels at the air-water interface more than at the organic interface.[19,46] The behavior of molecular anions such as $NO_3{}^-$ at H_2O/air has been explored recently with computer simulation,[28,48], spectroscopy,[49–51] and depth-resolved X-ray photoemission spectroscopy,[52]. Studies tend to agree that the air-water surface affinity of the $NO_3{}^-$ anion is no greater than the water bulk (i.e. for large simulated systems), but conclusions differ on the extent of density depletion or enhancement. The large planar geometry of the $NO_3{}^-$ anion and its low charge appear to repel it from the H_2O/air surface where it encounters a reduced solvent cage, and seeks a more hydrated solvation state. In comparison the $NO_3{}^-$ does alter the H_2O/CCl_4 interface with its density greatly enhanced within the surface region above bulk levels, and a wide ionic double-layer is established with its counter-ion left deeper in the aqueous bulk. It is likely that slight reorientation of the

surface waters near CCl_4 enhance the solvation of the $NO_3{}^-$ in the plane of the interface and establish a much more hydrated region for the anion to adsorb. Water reorientation is more fully described later in this work. The subsurface waters then continue to screen the charge of the surface-active $NO_3{}^-$, and decrease the coulombic force pulling the cation closer to the surface.

Unlike the monovalent ions, the divalent $SO_4{}^{2-}$ anion has a very large first solvation shell and has been found to prefer a location deeper into the aqueous phase at the H_2O/air interface,[44] and is perhaps repelled from the interfacial region.[53] This more highly-solvated anionic behavior coincides with the H_2O/CCl_4 system seen here. Although the presence of the CCl_4 changes the interfacial environment from that of the H_2O/air , the field established by the deep aqueous-side location of the $SO_4{}^{2-}$ anion density enhancement acts to affect the interface from a greater distance.

Ionic double-layers at both H_2O/air and H_2O/CCl_4 surfaces have been documented in many of the studies already referenced. The distance between the anion and cation subsurface enhancements at the H_2O/CCl_4 interface are shown in table 2. An SFG study by Schultz et al. noted the double-layer at the H_2O/air interface and attributed it to a "displacement" mechanism binding ions to interfacial waters, and forming contact-ion pairs. This was based on the lower-frequency OH vibrational mode found at 3150 cm^{-1} , and the lack of signal change with added salts. Since then Xu et al studied this phenomena finding no ion-pairing in solution of various nitrates with divalent cations at the H_2O/air interface.[50] The SFG study probed the vibrational modes of the $NO_3{}^-$ anion, rather than water's OH modes finding two anionic surface species. They concluded that solvation from an abundance of water at the interface weakens coulombic forces between ions, leading to greater cation-anion separation. The surface nitrate is dehydrated, and the water provides adequate shielding of the ionic coulombic interactions. In this work the ion double-layering at the H_2O/CCl_4 interface with no contact-ion pair formation for each of the salts. Likely, this is due to the stronger reorientation of water in the presence of the organic phase, and the subsequent field-screening by sub-surface waters between the ionic layers.

4 Water Orientation

Previous studies have provided a detailed overview of water orientation at the interface with both air and organic phases.[5,9,11,19,30] The topmost water layers are highly disrupted because of their contact with the organic phase, and it has been suggested that ordering of both the organic and water molecules would lead to a field across the boundary of the interface.[9,11] This can influence charged species, and the ordering and orientation of the H-bond network. Our recent experimental SFG results suggest that the accumulation of charged ions leads to a field-screening that affects the orientation of waters in the topmost layers. This is complemented by the results of the current study.

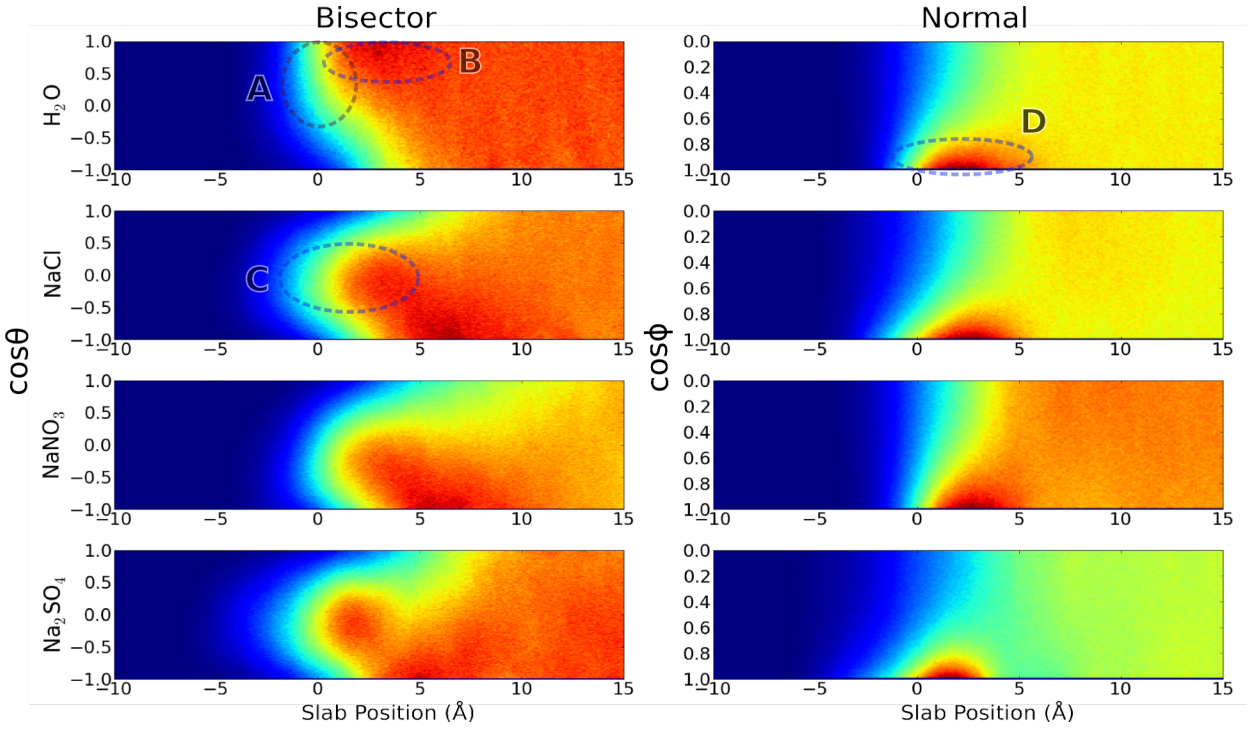

Figure. 3 — Orientation profiles of interfacial water molecules at different depths from the GDS. The molecular bisector profile (left column) and the profile of the molecular axis normal to the plane of the water molecule (right column) are shown. Both angle definitions are depicted in figure 1, and the angle cosines are plotted here. The neat-H_2O , NaCl , $NaNO_3$, and Na_2SO_4 system water orientation profiles are plotted from top to bottom row, respectively. Positive position values indicate the aqueous phase, and negative positions are in the CCl_4 phase. Regions labeled in the profile correspond to orientations depicted in figure 4.

The orientation of water within the aqueous/organic interface of the system was defined using the angles formed by molecular axes and the fixed reference axis of the system (perpendicular to the interfacial plane). The two molecular axes used are the water bisector, pointing from the hydrogen side to the oxygen, and the

vector normal to the plane formed by the three atoms of the water molecule, as depicted in figure 1. Figure 3 shows the angle profiles of both the molecular bisector and the molecular plane normal of water molecules relative to the system reference axis at various depths into the aqueous phase. Darker red regions of the plots indicate higher orientational populations, while homogeneous coloring across the angle range indicates orientational isotropy.

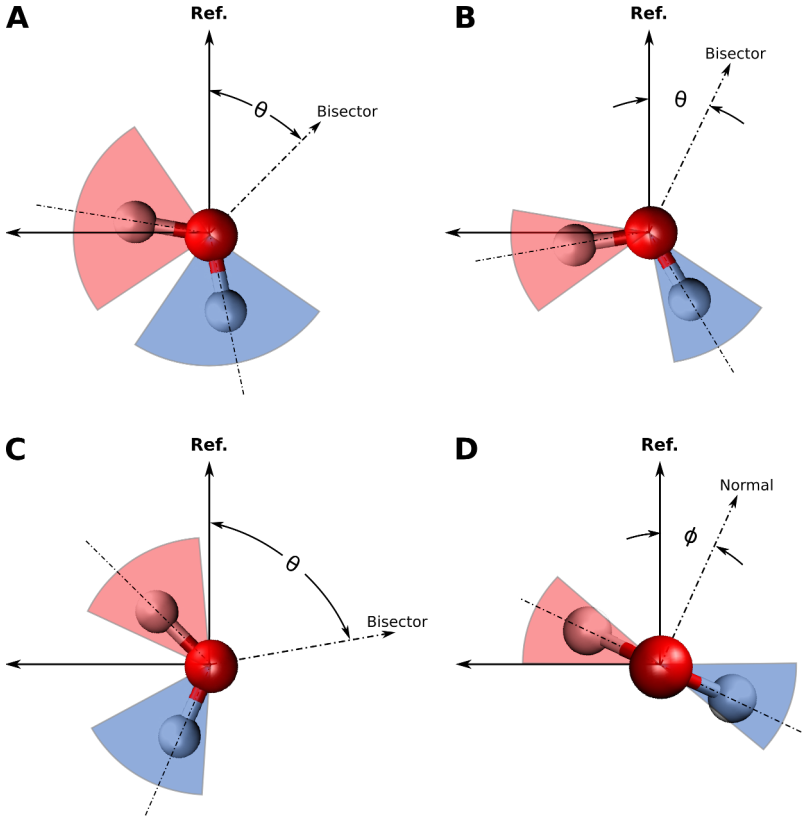

Figure. 4 — Depictions of water orientations ranges spanning varying values of θ and ϕ, as defined in figure 1. The effect of rotating the water within a fixed angle range is illustrated by the shaded (red and blue) regions that bound the OH-bonds. Ranges of θ shown here are (A) $0 < \cos\theta < 1$, (B) $0.7 < \cos\theta < 1$, (C) $-0.5 < \cos\theta < 0.5$. (D) The ϕ range of $0.7 < \cos\phi < 1$ shows the molecular plane of the water mostly flat (i.e. parallel to) the plane perpendicular to the reference axis. Depictions here correspond to those regions labeled in figure 3.

In the left column of figure 3 are the bisector orientation profiles for each of the systems. The far-left dark-blue regions of the plots show the CCl_4 bulk near to the interface where few or no waters are found. The GDS is located at a depth of 0.0 Å . To the far right in the water bulk, the flat, uniformly-colored profile represents the expected isotropic orientation of the waters. The regions of interest lie around the

GDS within the interface. The top bisector profile is that of the neat-H_2O system, and it shows a transition in the profile beginning a couple Å into the CCl_4 phase, and extending up to 5 Å into the aqueous side, at which point the profile becomes orientationally isotropic. At the GDS most of the waters are oriented between $0.0 < \cos\theta < 1.0$, indicating a range of orientation as depicted in figure 4a. In this range one of the OH-bonds points into the aqueous side, and the other straddles the interfacial plane with a slight affinity towards the organic CCl_4 phase. Just under the water surface, between 2-4 Å into the neat-H_2O phase, a dark-red region spanning approx. $0.7 < \cos\theta < 1.0$ appears. This narrow orientational range is depicted in figure 4b, and is similar to the waters in the topmost aqueous layer nearer to the GDS, but further limited such that one OH bond points into the H_2O side, and one of them only straddling the interfacial plane with a tendency to point into the H_2O phase.

The neat-H_2O bisector orientational profile is comparable to previous simulations of the same neat-H_2O reference system. Using different simulation parameters for the same neat-H_2O /CCl_4 system, Wick and Dang found the free-OH to point slightly into the CCl_4 phase at the GDS with an angle of $\cos\theta_{\ free-OH} \approx 0.4$. This corresponds to $\cos\theta_{\ bisector} \approx 0.5$ in the this work's angle definition. Similarly, deeper into the surface the angle profile diminishes such that $\cos(\theta_{free-OH}) \approx 0.0$ within 5 Å of the GDS, corresponding to $\cos(\theta_{bisector}) \approx 0.8$ in the current scheme. Those results agree with this work's neat-H_2O profile, further complementing the experimental SFG conclusions performed on the same systems.[9,54]

Bisector angle profiles for the salt systems show different behavior than that of the reference neat-H_2O system. The profiles of the salt systems at the GDS all center about the $\cos\theta = 0$ region, with a range of approx. $-0.5 < \cos\theta < 0.5$. This indicates a straddling water molecule with the orientational range depicted in figure 4c. The water in that range is clearly oriented such that one OH-bond always points out of the aqueous phase into the CCl_4 , and the other always points in to the water bulk. The OH-bond that would straddle the interface in the neat-water system points out of the interface with a greater angle. This orientation, centered about $\cos\theta \approx 0$, extends into the water phase up to 3 Å , at which point the profile shifts to the darker region near $-1.0 < \cos\theta < 0.7$. The sub-surface region of the profile between 4-7 Å in each system corresponds to a flip of the water orientation, as referred to in a recent SFG study as a "flip-flop" model where water orients to counteract the field of charged species at interfaces.[55] The cation density enhancement in each salt system is within the region of 5-7 Å below the GDS. The waters may be orienting with the negatively charged oxygen end towards those cations, and with the field established by the ion double-layer within the interface. In each of the salt bisector profiles there is a clear depletion of waters oriented towards $\cos\theta = 1$ suggesting that alignment of the bisector with the reference axis is not preferred. The effect is most pronounced in the Na_2SO_4 system where the distance between counter-ion density enhancements is smallest, and the transition in the bisector profile is the most abrupt, changing from a profile mostly in the range of $-1.0 < \cos\theta < 0.5$ to isotropic orientation quickly near 8 Å into the aqueous phase. The $NaNO_3$ system bisector profile shows the effect furthest into the water bulk, extending almost to 13 Å . Counter-ion density enhancement is most separated in $NaNO_3$, however, and most of the orientational affinity for $-1.0 < \cos\theta < 0.5$ occurs within the first 10 Å of the surface. The bisector profile

of the NaCl system is broadest with -1.0 $< \cos\theta <$ 0.7 starting near the GDS. Also, orientational isotropy is shallowest in the NaCl system starting near 7 Å into the aqueous phase.

It appears that the field established by the anion-cation pairing within the interface affects the depth to which waters are oriented before the bulk isotropic profile begins. Also, the range of orientations beneath the surface is dependent on the properties of the anion. The weakly polarizable Cl^- anion does not restrict the orientational range as much as the more polarizable ${NO_3}^-$ and ${SO_4}^{2-}$. Anions also appear to control the depth to which the water orientation is felt, with the most surface-active ${NO_3}^-$ anion causing the deepest effect. ${SO_4}^{2-}$ anion shows the strongest restriction on the range of bisector angles, and the sharpest orientational transition to the bulk, which may be attributed to the higher charge of the anion, and thus the stronger field established between the counter-ions in the system.

Orientational profiles for the molecular plane normal of the water molecules (ϕ-profiles) are found in the right-column of figure 3. The range of a ϕ-profile is limited to $0.0 < \cos\phi < 1.0$ because of the inherent symmetry of the plane of the water molecule. More similarity is shared between the ϕ-profiles than the bisector profiles for the different systems. The neat-H_2O profile is typical of the four profiles in appearance with a large clustering of water population in the range of $0.7 < \cos\phi < 1.0$ between the GDS and up to 7 Å into the aqueous phase. This particular ϕ range is depicted in figure 4d, showing the mostly flat (i.e. parallel to the interface) orientation of the molecular plane. It is notable that the ϕ-orientation is affected to the same depth as the first peak (dark-red region) of the bisector profile. However, in the salt systems the second peak near to $\cos\theta = -1.0$ begin at a depth where the ϕ-profile has already become isotropic. Thus, in the salt systems, the first water layer (between the GDS and almost 4 Å into the surface) has a defined ϕ-orientation that is rather flat on the interfacial plane, but the deeper waters (4-7 Å into the interface) are isotropic in ϕ, and oriented with $\cos\theta$ closer to -1.0 (an orientation with oxygen pointing into the water bulk, and hydrogens more towards the interface).

By virtue of the interdependence of θ and ϕ (the bisector is perpendicular to the molecular plane normal at all times) a value of $\cos\phi = 1.0$ implies $\cos\theta = 0$, and vice-versa. However, a broad θ-range allows for a full range of ϕ values. Although the second peak of the salt-system bisector profiles is concentrated near to $\cos\theta = -1.0$, the corresponding ϕ-profile is isotropic. This deeper region (the second water layer) orients with the bisector counteracting the field of the anion-cation double-layer, and the only apparent affinity is that of placing oxygen closer to the cation density enhancement (and hydrogen closer to the anion layer), while the ϕ-profile spans the entire orientational range.

5 Calculated Sum-Frequency Spectra

One of the aims of this simulation study is to provide complementary information to the SFG experimental studies of these systems.[9] The varied set of anions and their affect on the CCl_4 -H_2O interface is linked from theory to empirical data through the connection of computed SFG spectra. The computed spectra for the SSP polarization are presented in figure 5 along with the experimental spectra (inserts) from our previous work with these same salt solutions interfaced with CCl_4 .[9] Each of the spectra show both a salt system response (colored traces) overlayed on the reference H_2O/CCl_4 system spectrum (black or dashed-black traces). On first look, the overall computed intensities and lineshapes follow remarkably similar trends as in the experimental systems. All the spectra have a strong feature near 3660 cm^{-1} coinciding with the "free-OH" vibrations as defined previously, and corresponding to one of the uncoupled OH stretch modes from water molecules that "straddle" the interface (figure 1 a, b, and c).[9] The broad spectral region from 3200-3500 cm^{-1} is attributed to the more highly-coordinated OH-oscillators that are solvated at the surface, or just beneath the surface with stronger hydrogen-bonding. Each of the spectra computed for the salt-solutions differ markedly from each other and from the neat H_2O/CCl_4 spectrum. The monovalent ions (Cl^- and $NO_3{}^-$) in solution produce a measurable decrease in intensity of the lower-frequencies of the spectra with very little change to the free-OH mode. Like the experimental counterparts, the decrease is greatest around the 3200-3400 cm^{-1} region but shows little change from the neat-H_2O/CCl_4 system above 3500 cm^{-1} . Like in the SFG experiment, the presence of the $SO_4{}^{2-}$ anion causes an opposite effect by significantly enhancing the spectrum below 3600 cm^{-1} .

The reference CCl_4 -H_2O spectrum reproduces well the lineshape from experiment, but lacks the definition of the two peaks found near 3250 and 3450 cm^{-1} . These lower-frequency features have been attributed to the different H-bonding varieties of water that make up the more highly-coordinated, tetrahedral environments found deeper into the interfacial region. We have found difficulty in reproducing the lower-frequency peaks near 3200 cm^{-1} and attribute the slight differences in the lineshape to similar problems reported previously.[13] However, the neat-H_2O/CCl_4 lineshape is otherwise quite similar to that of the experiment. The salt solution signals spectra show an overall drop in signal from when Cl^- and $NO_3{}^-$ are added and an increase in intensity to $SO_4{}^{2-}$. This suggests that the methods are sound and justified for experimental comparison in this study.

The conclusions drawn from the experiments are that the presence of anions at the interface causes a "field-screening" that decreases the innate interfacial field at the organic/water interface, and consequently the number of bonded water molecules contributing to the SFG spectrum. Both the monovalent anions, Cl^- and $NO_3{}^-$, show this effect in their SFG spectra. For both experiment and these calculations, comparison to the reference neat-H_2O spectrum shows that the added presence of the surface-active anions decreases the lower-frequency intensities. Calculations show that Cl^- affects a notably smaller decrease in the spectral intensities than the $NO_3{}^-$ system, similar to experiment. This result is most likely due to the higher preference for the surface of the larger, and more polarizable nitrate in the presence of CCl_4 . The $NO_3{}^-$ ion is extremely surface active, as seen in the density profile, and should thus cause the greatest "field-screening"

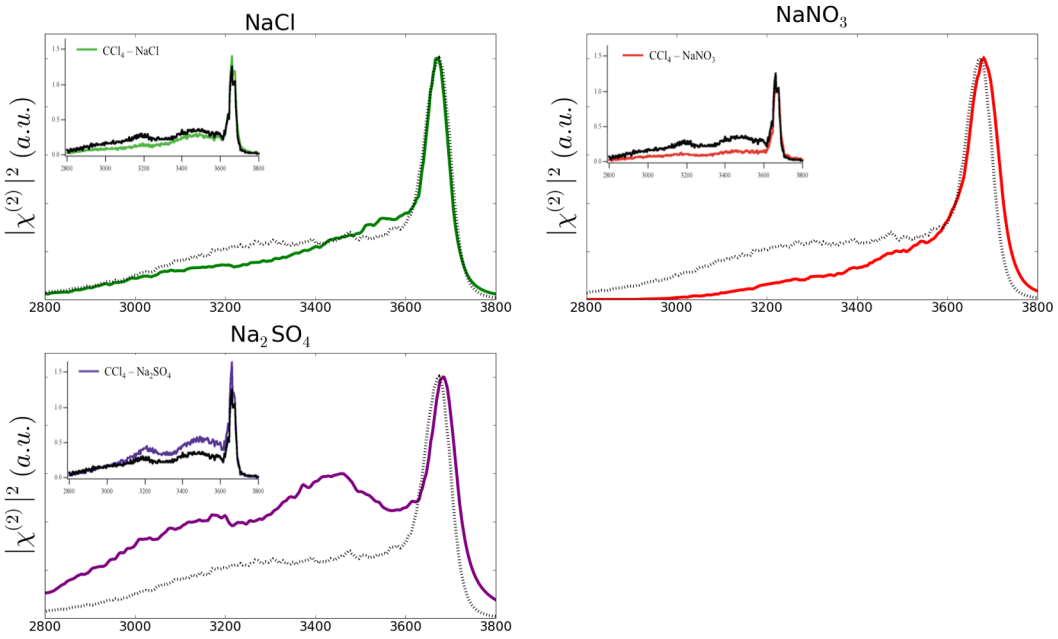

Figure. 5 — Vibrational SFG spectra of the water-OH stretching region for each interfacial aqueous-salt-CCl_4 system. The reference H_2O/CCl_4 interface spectrum (black-dashed line) is provided on each simulated SFG spectrum for reference. Inserts at the top left of each spectrum are reproductions of the experimental spectra from McFearin et al[9] including the reference (black) spectrum from that study. SSP polarization is used for all the spectra.

to waters found deeper in the bulk.

The divalent and larger ${SO_4}^{2-}$ anion accumulates deeper into the aqueous bulk and exhibits the lowest surface affinity of the ions studied. This is likely due to the higher charge of the anion that leads to greater solvation. The sulfate provides little or no screening of the interfacial field from the top-most water layer, and more greatly affects the deeper, highly-coordinated waters. The bonding region spanning the lower-frequency features is notably enhanced above the reference water signal in both experiment and computation. This indicates a stronger ordering of deeper waters, consistent with the anion location.

As concluded in the previous experimental work, the monovalent anions appear to screen the deeper water molecules from the field produced by the phase change at the aqueous-organic interface. This is supported by the confirmation through our MD simulations here that monovalent ions show a strong surface affinity and interact with surface waters. The large but more highly charged divalent ${SO_4}^{2-}$ anion experiences stronger solvation and is thus found deeper in the aqueous phase. Deeper anions do not participate as interfacial field screening agents to the same extent as their monovalent counterparts, but act to strongly orient the waters

near the interface, perhaps through the strong field established by the ion double-layering. The distance between the counter-ion density peaks (table 2) follows the inverse of the trend of SFG signal enhancement. As the ionic double-layer size increases, the SFG signal decreases. Similarly, the smallest double-layer size, that of the $SO_4{}^{2-}$ system, produces the greatest signal enhancement across the lower frequencies of the water OH-stretching SFG spectrum. Although the water density profiles do not change markedly between the different systems, the orientational profiles do show large variation from the neat-H_2O/CCl_4 system, and some slight variation between the salt-solutions. The two factors that may alter the SFG intensity of an experiment are changes in the number of contributing water bonded species, and a change in orientation of various water bonded species. From the water orientation profiles (figure 3) it is clear that the presence of anions at the H_2O/CCl_4 interface causes a strong orientation change from the reference H_2O/CCl_4 system. Thus we find that there appears to be a strong coupling between the presence and size of an ionic double-layer, subsequent reorientation of surface water molecules, and the resulting SFG signal change.

6 Conclusions

The unique environment created by interactions between water and hydrophobic molecules makes ionic adsorption and transport across interfaces possible. Aqueous-hydrophobic surfaces are of prime importance in applications ranging from ion transport, chemical remediation, and catalysis, to chemical synthesis. Complex interfaces between aqueous media and organic phases enhance chemical reactions, and this motivate further research to understand such environments. This study provides an important step in understanding aqueous-organic surfaces by computationally examining simple aqueous salt solutions interfaced with hydrophobic liquid CCl_4 . Through a combination of simulations and computational analysis, the nature of ionic adsorption and its effect on water hydrogen-bonding, geometry, and orientation at the liquid-liquid boundary is determined.

Analysis of the component density profiles provides a thorough microscopic picture of ionic surface affinity, double-layering, and effect on interfacial size. The smaller and less polarizable Cl^- anion behaves at the H_2O/CCl_4 surface much like at the H_2O/air interface, the larger surface-active anions do not. Density profile analysis shows that the $NO_3{}^-$ anion exhibits a much greater surface affinity near the organic phase than at an air interface, consistent with experiment. The orientational analysis of the solutions shows the very different effect of the various salts on the water orientation at the H_2O/CCl_4 boundary. The orientation profiles show a stratification of water geometries consistent with the emerging picture of a multi-layered surface region with varied geometries and interactions. This reorientation subsequently affects the ionic double-layering and subsurface waters. Such effects are manifested in spectroscopic changes to water's vibrational OH modes as seen in both the experimental and computational results. Consequently, SFG spectra computed in this study build the necessary bridge to our previous SFG work by offering direct comparison of the computational and experimental results. The surface spectroscopic signals, measured and calculated, are altered relative to the ion-free signal, indicating a change to the water bonding at the interface due primarily to the presence of the anion. The divalent $SO_4{}^{2-}$ anion acts to enhance the number and orientation of interface hydrogen-bonds, while the monovalent ions have a lessened effect, or decrease it. Both the organic phase and the salt anion species in solution contribute to altering the geometry and spectroscopy of water's surface.

We have thus moved toward our goal of further understanding the behavior and impact of ions and a hydrophobic phase on water at liquid-liquid interfaces. The complementing results of both simulation and experiment have strengthened our certainty of some of the underlying surface science of these systems, but challenges still remain. A more complete picture would include knowledge of different cation effects, as well as the changes to the surface by different hydrophobic phases. The ability to analyze these important interfacial environments both theoretically and experimentally now provides us with the tools to better develop our understanding them.

References

1. Charreteur, K.; Quentel, F.; Elleouet, C.; L'Her, M. *Analytical Chemistry* **2008,** *80,* 5065-5070.
2. Chen, X.; Yang, T.; Kataoka, S.; Cremer, P. S. *Journal of the American Chemical Society* **2007,** *129,* 12272-12279.
3. Luo, G.; Malkova, S.; Yoon, J.; Schultz, D.; Lin, B.; Meron, M.; Benjamin, I.; Vanysek, P.; Schlossman, M. *Science* **2006,** *311,* 216-218.
4. McArthur, E.; Eisenthal, K. *Journal of the American Chemical Society* **2006,** *128,* 1068-1069.
5. Wick, C. D.; Dang, L. X. *Chemical Physics Letters* **2008,** *458,* 1-5.
6. Schnell, B.; Schurhammer, R.; Wipff, G. *Journal of Physical Chemistry B* **2004,** *108,* 2285-2294.
7. Su, B.; Eugster, N.; Girault, H. *Journal of Electroanalytical Chemistry* **2005,** *577,* 187-196.
8. Wardle, K.; Henderson, D.; Rowley, R. *Fluid Phase Equilibria* **2005,** *233,* 96-102.
9. McFearin, C. L.; Richmond, G. L. *Journal of Physical Chemistry C* **2009,** *113,* 21162-21168.
10. Hore, D. K.; Walker, D. S.; MacKinnon, L.; Richmond, G. L. *Journal of Physical Chemistry C* **2007,** *111,* 8832-8842.
11. Hore, D. K.; Walker, D. S.; Richmond, G. L. *Journal of the American Chemical Society* **2008,** *130,* 1800+.
12. Hore, D. K.; Walker, D. S.; Richmond, G. L. *Journal of the American Chemical Society* **2007,** *129,* 752-753.
13. Walker, D. S.; Hore, D. K.; Richmond, G. L. *Journal of Physical Chemistry B* **2006,** *110,* 20451-20459.
14. Walker, D. S.; Richmond, G. L. *Journal of the American Chemical Society* **2007,** *129,* 9446-9451.
15. Walker, D. S.; Moore, F. G.; Richmond, G. L. *Journal of Physical Chemistry C* **2007,** *111,* 6103-6112.
16. Chang, T.; Peterson, K.; Dang, L. *Journal of Chemical Physics* **1995,** *103,* 7502-7513.
17. Eggimann, B. L.; Siepmann, J. I. *Journal of Physical Chemistry C* **2008,** *112,* 210-218.
18. Du, H.; Liu, J.; Ozdemir, O.; Nguyen, A. V.; Miller, J. D. *Journal of Colloid and Interface Science* **2008,** *318,* 271-277.
19. Wick, C.; Dang, L. *Journal of Physical Chemistry B* **2006,** *110,* 6824-6831.

20. Petersen, P.; Saykally, R.; Mucha, M.; Jungwirth, P. *Journal of Physical Chemistry B* **2005,** *109,* 10915-10921.

21. Matsumoto, M.; Kataoka, Y. *Journal of Chemical Physics* **1988,** *88,* 3233-3245 hyperbolic tangent fitting function for water density profiles.

22. Petersen, P.; Saykally, R. *Annual Review of Physics Chemistry* **2006,** *57,* 333-364.

23. Allen, H. C.; Casillas-Ituarte, N. N.; Sierra-Hernandez, M. R.; Chen, X.; Tang, C. Y. *Physical Chemistry Chemical Physics* **2009,** *11,* 5538-5549.

24. Hofft, O.; Borodin, A.; Kahnert, U.; Kempter, V.; Dang, L.; Jungwirth, P. *Journal of Physical Chemistry B* **2006,** *110,* 11971-11976.

25. Beattie, J.; Djerdjev, A.; Franks, G.; Warr, G. *Journal of Physical Chemistry B* **2005,** *109,* 15675-15676.

26. Bian, H.-t.; Feng, R.-r.; Guo, Y.; Wang, H.-f. *Journal of Chemical Physics* **2009,** *130,*.

27. Dang, L. *Abstracts of Papers of the American Chemical Society* **2004,** *228,* 86-PHYS.

28. Thomas, J. L.; Roeselova, M.; Dang, L. X.; Tobias, D. J. *Journal of Physical Chemistry A* **2007,** *111(16),* 3091-3098.

29. Wick, C. D.; Kuo, I.-F. W.; Mundy, C. J.; Dang, L. X. *Journal of Chemical Theory and Computation* **2007,** *3,* 2002-2010.

30. Fan, Y.; Chen, X.; Yang, L.; Cremer, P. S.; Gao, Y. Q. *Journal of Physical Chemistry B* **2009,** *113,* 11672-11679.

31. Galamba, N.; Cabral, B. J. C. *Journal of the American Chemical Society* **2008,** *130,* 17955-17960.

32. Ishiyama, T.; Morita, A. *Journal Of Physical Chemistry C* **2007,** *111,* 738–748.

33. Morita, A.; Hynes, J. *Chemical Physics* **2000,** *258,* 371-390.

34. Walker, D. S.; Richmond, G. L. *Journal of Physical Chemistry C* **2008,** *112,* 201-209.

35. Morita, A.; Hynes, J. *Journal of Physical Chemistry B* **2002,** *106,* 673-685.

36. Ishiyama, T.; Morita, A. *Journal of Physical Chemistry C* **2009,** *113,* 16299-16302.

37. Chang, T.; Dang, L. *Journal of Physical Chemistry B* **1997,** *101,* 10518-10526.

38. Dang, L. *Journal of Physical Chemistry B* **1999,** *103,* 8195-8200.

39. Hrobarik, T.; Vrbka, L.; Jungwirth, P. *Biophysical Chemistry* **2006,** *124,* 238-242.

40. Caldwell, J. W.; Kollman, P. A. *J. Phys. Chem.* **1995,** *99,* 6208-6219.

41. Rivera, J. L.; Starr, F. W.; Paricaud, P.; Cummings, P. T. *Journal of Chemical Physics* **2006,** *125,*.

42. Petersen, P.; Saykally, R. *Journal of the American Chemical Society* **2005,** *127,* 15446-15452.

43. Dang, L. *Journal of Physical Chemistry B* **1998,** *102,* 620-624.

44. Salvador, P.; Curtis, J. E.; Tobias, D. J.; Jungwirth, P. *Physical Chemistry Chemical Physics* **2003,** *5,* 3752–3757.

45. Chang, T.; Dang, L. *Journal of Chemical Physics* **1996,** *104,* 6772-6783.

46. Wick, C.; Dang, L. X. *Journal of Chemical Physics* **2007,** *126,*.

47. Jungwirth, P.; Hoefft, O.; Kahnert, U.; Kempter, V.; Dang, L. X. *Abstracts of Papers of the American Chemical Society* **2006,** *231,*.

48. Miller, Y.; Thomas, J. L.; Kemp, D. D.; Finlayson-Pitts, B. J.; Gordon, M. S.; Tobias, D. J.; Gerber, R. B. *JOURNAL OF PHYSICAL CHEMISTRY A* **2009,** *113,* 12805-12814.

49. Otten, D. E.; Petersen, P. B.; Saykally, R. J. *Chemical Physics Letters* **2007,** *449,* 261-265.

50. Xu, M.; Tang, C. Y.; Jubb, A. M.; Chen, X.; Allen, H. C. *Journal of Physical Chemistry C* **2009,** *113,* 2082-2087.

51. Soule, M. C. K.; Blower, P. G.; Richmond, G. L. *Journal Of Physical Chemistry A* **2007,** *111,* 3349–3357.

52. Brown, M. A.; Winter, B.; Faubel, M.; Hemminger, J. C. *Journal of the American Chemical Society* **2009,** *131,* 8354.

53. Gopalakrishnan, S.; Jungwirth, P.; Tobias, D.; Allen, H. *Journal of Physical Chemistry B* **2005,** *109,* 8861-8872.

54. Scatena, L.; Richmond, G. *Journal of Physical Chemistry B* **2001,** *105,* 11240-11250.

55. Nihonyanagi, S.; Yamaguchi, S.; Tahara, T. *Journal of Chemical Physics* **2009,** *130,*.